Econ. Environ. Geol.
Vol. 30, No. 5, p. 477-491, 1997.

Genetic Implications of Ultramafic Rocks from the Bibong Area in the Kyeonggi Gneiss Complex*

Suck Hwan Song, Seon Gyu Choi** and Jun Gie Woo****

ABSTRACT : In the Bibong area of the western part of Chungcheongnam-do, ultramafic masses occur as discontinuous isolated lenticular bodies in the Precambrian Kyeonggi gneiss complex. They extend for about 200 m long to NNE directions which are parallel to fault lines in the gneiss complex. The ultramafic masses contact with the adjacent gneiss complex as steeply dipping faults. They are dunites and harzburgites and many of them are partially or completely serpentinized. The ultramafic rocks dominantly show protogranular, equigranular and equigranular-mosaic textures. They also show porphyroclastic (megacrystic) or recrystallized textures reflecting several stages of metamorphism. They contain varying amounts of olivine (Fo_{89-92}), enstatitic to bronzitic orthopyroxene, diopsidic clinopyroxene, tremolitic to pargasitic hornblende, and spinel with serpentine, talc, chlorite, calcite and magnetite. The ultramafic rocks have high magnesium numbers and transitional element contents, low alkali contents and show deplete REE patterns. Comparing with available data, geochemical and mineralogical characteristics shown in the ultramafic rocks of the Bibong area are similar to those of worldwide mantle xenoliths and orogenic related ultramafic rocks. The field evidences, petrographical, geochemical and mineralogical characteristics shown in the ultramafic rocks of the Bibong area are similar to alpine type ultramafic rocks emplaced into the crust by the faulting as mantle slab types. With the petrographical characteristics, these mineralogical compositions suggest that the ultramafic rocks of the Bibong area have experienced several stages of retrogressive metamorphism in a condition ranging from the upper amphibolite facies to greenschist facies.

INTRODUCTION

Exposed ultramafic rocks provide important key to understand nature, formation, and evolution of the lower crust and upper mantle levels (Frey *et al.*, 1974; O'Reilly *et al.*, 1988; Jackson, 1991). They occur as xenoliths in basalts, kimberlites and lamprophyres (Boyd *et al.*, 1975; Griffin *et al.*, 1984; O'Reilly, Griffin, 1988) as well as irregular and elliptical bodies exposed by orogenic movements (Loomis, 1972; Christen, Lundquist, 1982; Nicolas, Viollette, 1982, Rampone *et al.*, 1995). The orogenic related ultramafic bodies have been known as alpine type ultramafic rocks (Hess, 1955; Den Tex, 1969; Moores, MacGregor, 1972).

The ultramafic rocks of alpine type occur to be related to present or previous plate boundaries (Hamlyn, Bonatti, 1980; Nicolas, 1986; Girardeau, Mercier, 1980). They expose within Phanerozoic mountain belts (Moores, Jackson, 1974; Hebert *et al.*, 1989; Mittwede, Stoddard, 1989; Spell, Norrel, 1990) as well as Precambrian terrains (Nutman *et al.*, 1984; Dymek *et al.*, 1988). Thus, their studies can provide a wealth of information relevant to the tectonic setting and thermal evolution of ancient orogenies (Dymek *et al.*, 1988; Raymond, 1995).

Several worldwide studies suggest evidences for multiple episodes of deformation or metamorphism within the ultramafic rocks (Pakdung, 1984; Dymek *et al.*, 1988). Thus early formative and emplacement events of the ultramafic rocks can be commonly obscured by the subsequent metamorphism after emplaced into the crust by the faulting (Raymond, 1995).

In Korea, the ultramafic rocks mainly occur at western part of Chungcheongnam-do, Cheongyang and Hongseong areas, with southeastern part of Korean peninsula, Andong and Ulsan areas (Ji, Kim, 1977; Choi, 1988; Kim *et al.*, 1990; Woo *et al.*, 1991; Hwang *et al.*, 1993; Wee *et al.*, 1994; Yun *et al.*, 1994). They mainly occur as discontinuously isolated bodies along the regular directions. The ultramafic rocks from the Cheongyang and Hongseong areas are several ten to hundred meters in length and dominantly occur as fault contacts with adjacent Precambrian metamorphic and metasedimentary rocks.

* Present studies were supported in part by the Basic Sicence Research Institute Program, Ministry of Education, 1996, Project No. BSRI-94-5403.

** Department of Earth and Environmental Sciences, Korea University, Seoul 136-701, Korea.

At the Bibong area, three ultramafic masses, Bibong, Migok and Kwangsi, are distributed along the NNE direction. Among the three masses, the Bibong mass is still exploited. General geology of the Bibong area was provided by several studies (Lee, Kim, 1963; Eum, Lee, 1963). Several studies also provided for the ultramafic rocks in the respect of genesis of talc and vermiculite deposits (Song, Moon, 1991; Woo *et al.*, 1991; Yun *et al.*, 1994) as well as for petrochemical studies (Wee *et al.*, 1994). The genetic approaches suggest that talcification of the talc deposits was formed from serpentinites with subsequent metamorphisms, deformations and hydrothermal alterations. The petrochemical approaches suggest that the ultramafic rocks were residuals of upper mantle partially melted.

This study is mainly concerned with genetic implications of the Kwangsi and Bibong ultramafic masses. Mineralogical and geochemical approaches are tried to interpret for origin and nature of the ultramafic suites. In addition, metamorphism and deformation episodes after or during their emplacements are also considered. All these results were compared with those of worldwide tectonic related ultramafic rocks.

GELOGICAL SETTING

General geology

The studied area consists of Precambrian gneiss complex and metasediment, Mesozoic sedimentary strata, and their intrusive rocks (Fig. 1, Lee, Kim, 1963; Eum, Lee, 1963). The Precambrian gneiss complexes were intruded by age-unknown aplitic granite gneiss. However, no relationships are found between aplitic granite gneiss and the other rock types.

The gneiss complex is a basement in this area, and composed of biotite-, banded- and augen gneisses. They locally show gradational variation. They show dominantly N 20~40° E strike and 30~50° SE dip in

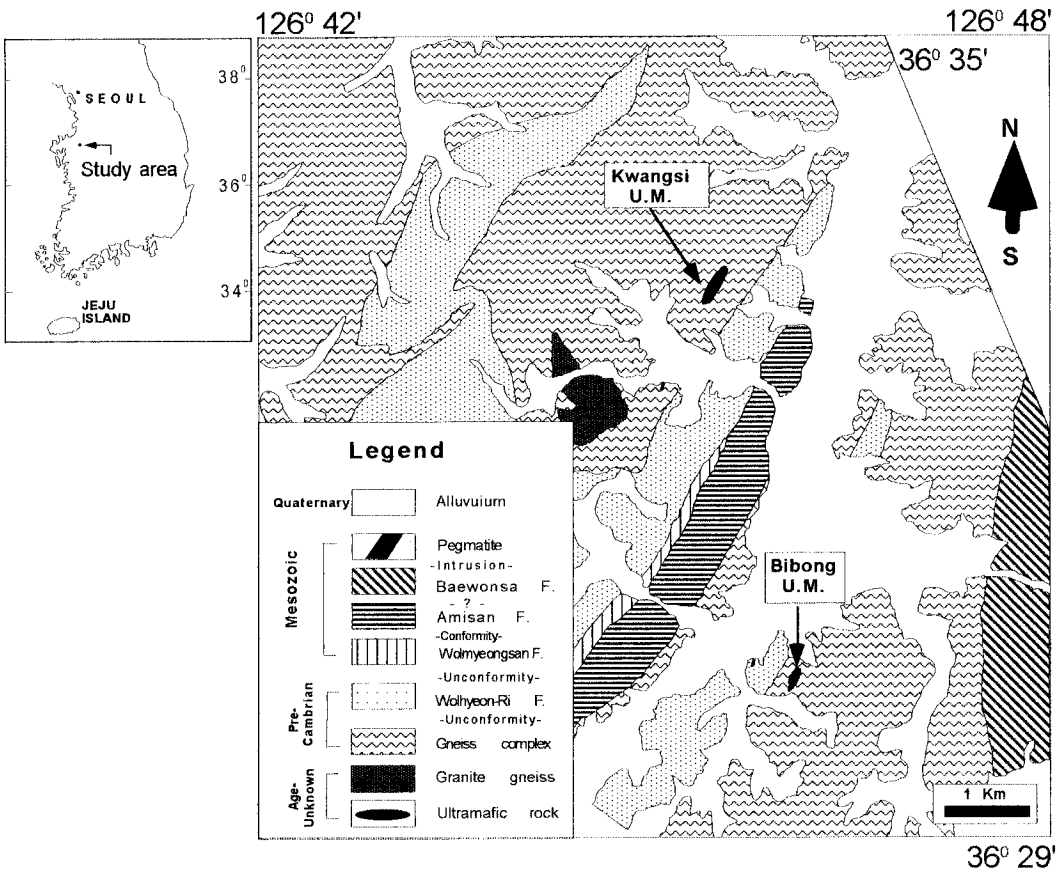

Fig. 1. Geological map of the Bibong area.

gneissosity. The augen gneiss is characterized by alkali-feldspar porphyroclasts (1~5 cm in diameter) and banded gneiss is characterized by alternative bands (1~3 cm in size), leucocratic and melanocratic bands. The gneiss contains quartz, plagioclase, alkali-feldspar, biotite, amphibole, garnet, chlorite with minor sillimanite, apatite, zircon and magnetite.

The Weolhyunri Formation consists of biotite-, biotite and amphibole- schists and metabasites. The schists are unconformably underlain by the gneiss complex whereas the metabasites are found within the gneiss and schist. However, no relationships are found between the schist and metabasite. The schists show N 32~50° E strike and 40~60° SE dip. The schists contain quartz, plagioclase, alkali-feldspar, biotite, amphibole, garnet, muscovite with minor magnetite, hematite, apatite and zircon, which are well aligned to the distinct directions of schistosity. The metabasites are divided into two types; one containing amphibole, biotite, quartz and plagioclase with minor quartz, magnetite, hematite and showing equigranular and mosaic textures whereas the other containing garnet, amphibole, biotite and plagioclase with minor quartz, magnetite, spinel, hematite and showing decompressive and recrystallization textures. The latters show garnets rimmed by amphibole and clinopyroxene and subsequently by quartz, plagioclase and epidote as well as amphiboles rimmed by biotite, subsequently by quartz. These texture suggests retrogressive metamorphism. The metabasites also contain coarse grained amphiboles marginally recrystallized to fine granular grains.

The Weolmyungsan Formation is the lowest unit of Mesozoic sediment strata and unconformably underlain by the Weolhyunri Formation. It shows N 30~45° E strike and 40~60° SE dip and consists of conglomerate, black sandstone, black and coaly shale, and coal seam. The sandstone partly shows a gradational variation, from sand to gravel, in grain sizes. The conglomerate contains well rounded pebbles (0.5~20 cm in diameter) from the various rock types and has quartz, biotite with plagioclase, microcline, muscovite and magnetite whereas the sandstone contains quartz and microcline with plagioclase, muscovite, biotite and magnetite. The black and coal-bearing shales contain quartz, biotite, amphibole and plagioclase with minor graphite, magnetite and zircon.

The Amisan Formation is conformably underlain by the Weolmyungsan Formation. It dominantly shows N 20~30° E strike and 50~80° SE dip and is composed of medium grained black and coal bearing shales. The black shale is composed of coal material, quartz, biotite, alkali-feldspar, plagioclase and magne- tite with zircon.

The Baekwonsa Formation occurs at eastside of the study area and is unconformably underlain by the Precambrian gneiss complex. No stratigraphic relationships are found with the other Mesozoic sedimentary rocks. It is composed of black sandstone, black shale, conglomerate, conglomeratic sandstone and coal bearing layer. They show dominantly N 30~40° E strike and 60~80° NW dip directions. The sandstone is dominant in this area and contains quartz, feldspar, mica and clastic rock fragments. The black shale contains quartz, alkali-feldspar, plagioclase and muscovite with magnetite, monazite, coal material and zircon. The conglomerate contains round to subround pebbles (mainly 3~8 cm in diameter) composed of sandstone, lime silicate, shale, granitoid and schist. The coal occurs as seams and as lense shapes within the back shale.

The aplitic granite gneiss occurs at southwest of the Kwangsi mass and contain plagioclase, K-feldspar, biotite, quartz with minor amphibole and magnetite. The Late Jurassic to Cretaceous plutonic rocks are pink feldspar granite, pegmatite, aplitic rock and hornblendite in 0.8~2 m diameter with other fine vein shaped dykes.

Descriptions of the ultramafic rocks

The ultramafic rocks occur as extended lense shapes and contact with the Precambrian gneiss complex as a steeply dipping fault. Their distributions are NNE directions which are parallel to general directions of structural frameworks (ex. fault) in this area. The Bibong ultramafic rock is about 250 m long and extends to N 20~35° E direction. The Kwangsi ultramafic rock is about 180 m long and extends to N 20~40° E direction. The ultramafic rocks show slightly deviate strike comparing with that of the adjacent gneiss complex and are found within adjacent country rocks as large allogenetic blocks, suggestive of movements after emplacement of the ultramafic rocks.

The ultramafic rocks are dunite and harzburgite. They contain varying amounts of olivine, orthopyroxene, clinopyroxene and spinel with serpentine, talc, chlorite, amphibole, calcite and magnetite. The rocks dominantly show protogranular, equigranular-mosaic and equigranular-tabular textures (Fig. 2).

They are serpentinized to the direction of the emplacements. Their serpentinized bands are several to tenth centimeters. The ultramafic rocks are also altered by the several stages of igneous intrusive rocks and intrusion of the vermiculate veins. The alterations are characterized by serpentinization, chloritization and talcification. The serpentinization occurs after olivine and orthopyroxene. The chlo- ritization occurs after orthopyroxene, amphibole and phlogopite whereas the

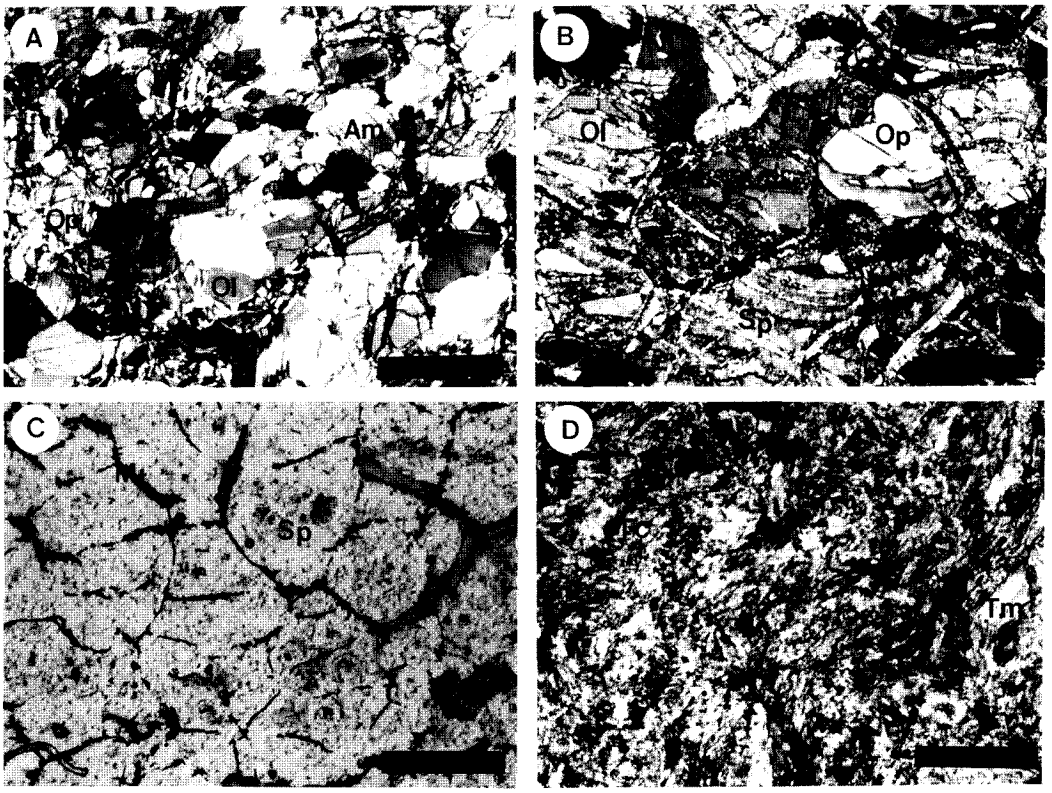

Fig. 2. Photomicrograpies of four ultramafic types from the Bibong area: A) peridotite (PD) contains olivine (Ol), orthopyroxene (Op), amphibole (Am) with minor magnetite and serpentine. This type only contain serpentines less than 15%; B) partly serpentinized peridotite (PSP) contains serpentines (Sp) ranging from 15 to 75%, with olivine (Ol), orthopyroxene (Op) and amphibole; C) serpentinite (SP) contains serpentine (Sp) and magnetite (Mt) with minor chlorite and tremolite. This type do not contain olivine and pyroxene; D) talcified rock (TC) only contains talc (Tc) with minor tremolite (Tm), chlorite (Ch) and magnetite. Width of a scale bar is 0.5 millimeter.

talcification occurs after serpentine formed olivine and othopyroxene or chlorite formed from phlogopite and amphibole.

In this study, the ultramafic rocks are divided into two types; peridotite and serpentinized rocks. The serpentinized rocks are divided into three types; partly sepertinized peridotite, serpentinite and talcified rock. The peridotite (PD) is referred as a rock type which mainly consists of olivine and orthopyroxene with amphibole and magnetite. They contain serpentines less than 15%. The partly serpentinized peridotite (PSP) is referred as a rock type containing serpentines ranging from 15 to 75%. The serpentinite (SP) contains only serpentines and magnetites with minor chlorite. The talcified rock (TC) mostly contains talc with minor serpentine, magnetite, tremolite and chlorite.

METHODS OF INVESTIGATIONS

Samples of the ultramafic rocks were collected according to several occurrence types at the Bibong area. Samples were also collected to the adjacent Precambrian metamorphic and metasedimentary rocks with vermiculate veins. Selected sixteen samples were analysed to determine major and trace elements, and REE by the ICP and ICP/MS of ACTLABS, Canada. Mineral compositions were determined on energy dispersive spectrometer (EDS) attached to the JEOL 8600 electron microprobe of the Korea University (15 kV accelerating voltage, 20 nA beam current and 10 micro beam diameter).

WHOLE ROCK GEOCHEMISTRY

Ultramafic rocks

Major and transitional elements; All major and transitional element analyses of the ultramafic rocks show in Table 1 and 2. The ultramafic rocks have high magnesium numbers (=100*Mg/(Mg+Fe(total),

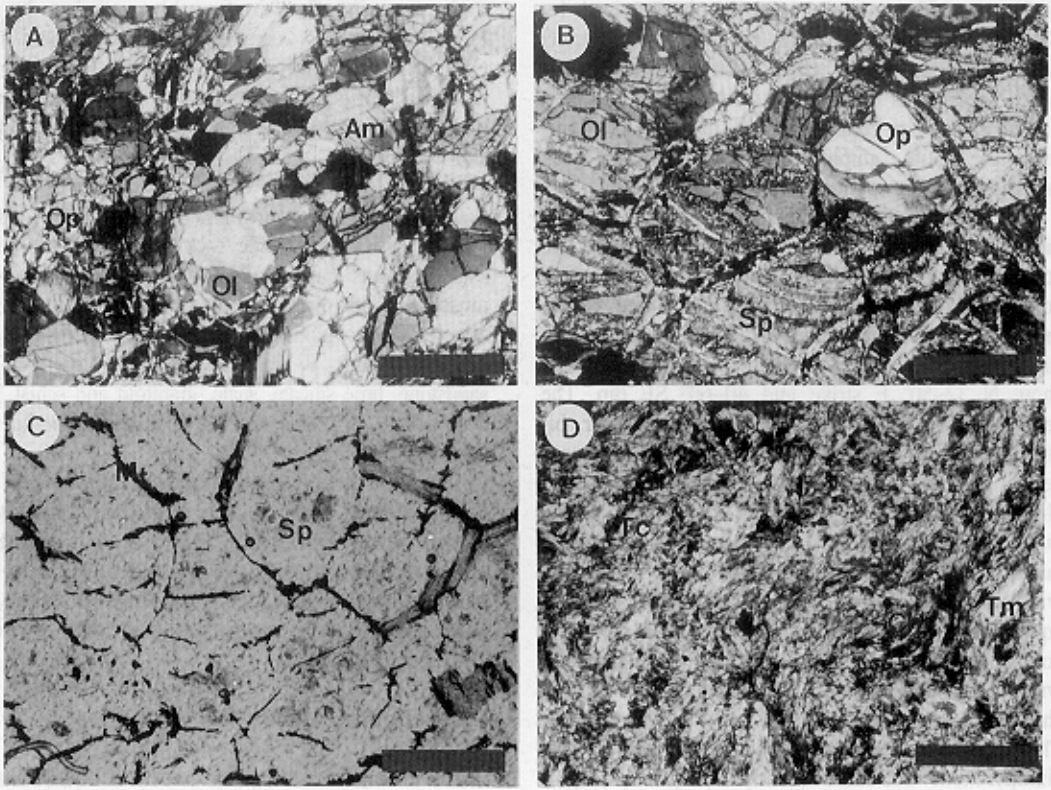

Fig. 2. Photomicrographies of four ultramafic types from the Bibong area: A) peridotite (PD) contains olivine (Ol), orthopyroxene (Op), amphibole (Am) with minor magnetite and serpentine. This type only contain serpentines less than 15%; B) partly serpentinized peridotite (PSP) contains serpentines (Sp) ranging from 15 to 75%, with olivine (Ol), orthopyroxene (Op) and amphibole; C) serpentinite (SP) contains serpentine (Sp) and magnetite (Mt) with minor chlorite and tremolite. This type do not contain olivine and pyroxene; D) talcified rock (TC) only contains talc (Tc) with minor tremolite (Tm), chlorite (Ch) and magnetite. Width of a scale bar is 0.5 millimeter.

Table 1. Major element analyses of the ultramafic and their related rocks from the Bibong area.

Loacality	Bibong										Kwangsi					
Type	PSP						TC	VM	MB	GN	PD		PSP	SP	MB	GN
Name	BB1-7	BB1-8	BB1-10	BB1-11	BB1-1	BB1-9	BB1-4	BB4-3D	KS8-6	KS6-3	KS8-3	KS8-1	KS8-2	KS8-4	KS8-06	KS8-7
SiO_2	38.21	38.91	39.00	39.57	39.47	38.56	49.44	47.04	46.80	71.71	40.93	41.13	39.77	36.84	48.28	72.85
TiO_2	0.01	0.02	0.02	0.01	–	0.08	0.08	1.08	0.24	0.75	0.11	0.12	0.01	–	0.75	0.13
Al_2O_3	0.68	1.03	0.46	0.45	0.76	0.56	4.12	14.50	16.29	13.26	2.92	3.32	0.82	0.33	13.98	11.86
Fe_2O_3*	8.00	7.61	7.82	7.68	5.75	8.29	7.30	15.73	9.59	5.67	8.32	7.00	6.92	8.98	11.46	2.54
MnO	0.11	0.10	0.10	0.10	0.07	0.05	0.16	0.16	0.13	0.08	0.11	0.10	0.07	0.07	0.16	0.04
MgO	42.14	41.09	42.09	42.72	40.30	39.37	24.08	7.44	11.47	1.87	39.03	34.72	39.76	39.05	8.78	1.19
CaO	0.57	0.89	0.35	0.34	0.03	0.29	8.81	9.23	12.95	1.55	2.22	.91	0.17	0.06	12.32	0.71
Na_2O	0.01	0.05	0.03	–	0.01	–	0.05	1.88	1.52	2.09	0.22	0.24	0.07	–	2.91	3.01
K_2O	–	0.03	0.03	0.03	0.02	0.01	0.06	2.04	0.45	2.96	0.02	0.08	–	–	0.26	4.88
P_2O_5	0.02	–	–	–	–	–	–	0.23	0.01	0.11	0.02	–	–	–	0.07	0.02
LOI	9.91	10.21	10.40	9.72	12.90	12.36	5.29	1.30	1.23	0.69	8.16	10.56	12.54	12.47	0.71	0.81
Total	99.65	99.94	100.31	100.64	99.32	99.49	99.40	100.63	100.68	100.73	100.07	100.07	100.13	99.62	99.69	98.04

Abbreviations are the same as those in the Fig. 2 exclusive of following: VM; vermiculate vein, MB; metabasite and GN; gneiss. Fe_2O_3* is total iron. – means elements not detected.

Mg) ranging from 87 to 92 and low alkali ($K_2O < 0.02$ wt%, $Na_2O < 0.24$ wt%) and TiO_2 (< 0.12 wt%) contents (Table 1). However, clear geochemical distinctions are found among the rock types showing different degrees of alteration. The TC shows highest SiO_2 (49.44 wt%), Al_2O_3 (4.12 wt%) and, CaO (8.81 wt%) contents and lowest *Mg* (86.7) among the four ultramafic varieties. The PD shows higher Al_2O_3 (2.9~3.3 wt%), CaO (1.9~2.2 wt%) and Na_2O (0.22~0.24 wt%) contents than the PSP and SP. The SP has lower K_2O, CaO and MnO contents than the PSP.

Except the TC, the ultramafic rocks contain high Ni (> 2450 ppm), Cr (> 1600 ppm), and Co (> 80 ppm), and low Sc (< 12 ppm), V (< 62 ppm) and Zn (< 63 ppm) contents. But, no clear geochemical distinctions are recognized among rocks showing varying degrees of alterations in the transitional

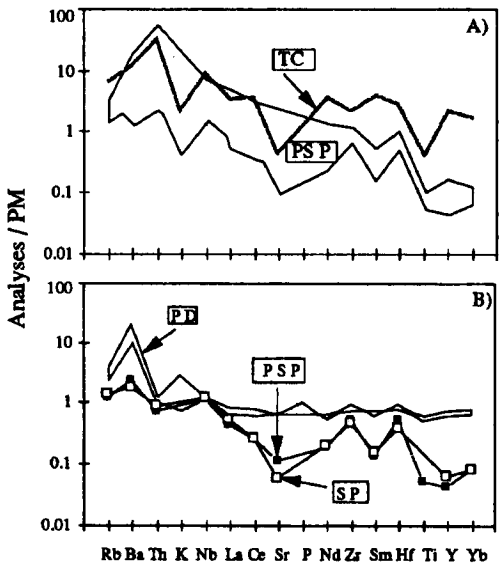

Fig. 3. PM (primitive mantle) composition normalized incompatible element abundances of Bibong (A) and Kwangsi (B) ultramafic rocks. Abbreviations are in the Fig. 2. PM data from Sun, McDonough (1989).

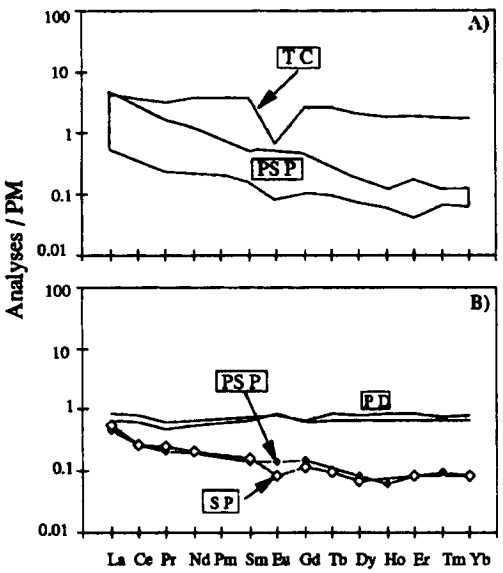

Fig. 4. PM composition normalized REE abundances of Bibong (A) and Kwangsi (B) ultramafic rocks. Abbreviations are in the Fig. 2. PM data from Sun, McDonough (1989).

Table 2. Trace elemnent analyses of the ultramafic and their related rocks from the Bibong area (in ppm).

Locality	Bibong										Kwangsi					
Type	PSP						TC	VM	MB	GN	PD		PSP	SP	MB	GN
Name	BB1-7	BB1-8	BB1-10	BB1-11	BB1-1	BB1-9	BB1-4	BB4-3D	KS8-6	KS6-3	KS8-3	KS8-1	KS8-2	KS8-4	KS8-06	KS8-7
Ni	2871	2847	2789	2909	3005	2465	1014	67	263	44	2462	2515	2826	2949	180	152
Cr	2385	1895	2159	1842	2616	1689	911	322	466	118	1900	2189	2224	1620	343	60
Co	108	104	103	107	101	79	65	40	50	12	100	103	93	117	54	5
Sc	6.0	6.0	5.0	5.0	6.0	6.0	6.0	34.0	33.0	12.0	12.0	12.0	4.0	4.0	42.0	2.0
V	28.0	30.0	20.0	19.0	33.0	24.0	20.0	201.0	139.0	90.0	63.0	71.0	27.0	18.0	288.0	6.0
Cs	0.12		0.15	0.21	0.09	0.06	1.10	3.13	0.80	1.83	0.11	0.44	0.07	0.13	0.23	0.70
Ba	17.8	0.08	133.6	8.5	17.8	64.5	84.4	501.6	39.8	632.9	138.5	67.8	16.5	13.3	108.1	638.3
Sr	6.5	61.0	10.5	3.6	1.4	2.3	9.5	63.8	151.5	15.1	15.1	14.6	2.5	1.2	132.1	176.3
Rb	0.93		1.69	2.03	1.21	1.06	4.15	161.1	8.5	85.9	1.55	2.5	0.78	0.89	8.94	157.11
Zr	12.3	11.3	7.6	12.3	12.9	7.0	22.8	416.6	15.8	296.7	11.2	9.0	6.2	5.5	41.5	277.3
Nb	5.2		1.5	1.1	2.6	1.1	6.8	11.6	31.4	14.1	0.8	0.8	0.8	0.9	1.6	29.5
Y	0.20	1.22	0.50	0.40	0.70	0.20	8.5	46.8	8.0	29.0	2.9	3.5	0.20	0.30	24.9	99.6
Ta	0.09	9.8	0.07	0.05	0.16	0.06	0.65	0.58	0.09	0.83	0.04	0.04	0.02	0.04	0.07	2.07
La	0.36	1.7	1.02	0.52	3.12	1.02	2.20	51.47	1.12	33.21	0.45	0.58	0.30	0.37	2.50	57.14
Ce	0.62	0.40	1.92	1.06	5.20	1.25	6.55	107.49	2.15	62.08	1.11	1.44	0.47	0.48	2.78	134.02
Pr	0.07	0.07	0.20	0.10	0.44	0.10	0.87	10.08	0.31	2.97	0.13	0.17	0.06	0.07	0.55	11.87
Nd	0.06	0.47	0.84	0.43	1.67	0.40	5.08	47.24	1.95	28.01	0.73	0.87	0.26	0.28	4.11	59.55
Sm	0.08	0.81	0.13	0.07	0.23	0.07	1.569	8.40	0.74	5.13	0.29	0.34	0.06	0.07	1.70	14.27
Eu	0.01	0.08	0.07	0.03	0.09	0.09	0.12	1.53	0.43	1.49	0.14	0.13	0.02	0.01	0.60	1.04
Gd	0.06	0.35	0.15	0.11	0.28	0.28	1.53	9.74	0.86	5.76	0.37	0.40	0.09	0.07	2.36	15.13
Tb	0.01	0.10	0.22	0.02	0.03	0.03	0.28	1.45	0.19	0.83	0.07	0.09	0.01	0.01	0.63	2.89
Dy	0.05	0.03	0.10	0.09	0.13	0.13	1.53	7.85	1.21	4.49	0.48	0.60	0.06	0.05	4.05	17.90
Ho	0.01	0.10	0.01	0.01	0.02	0.02	0.31	1.61	0.27	0.98	0.11	0.14	0.01	–	0.87	3.69
Er	0.02	0.02	0.04	0.04	0.08	0.08	0.94	4.86	0.87	3.33	0.32	0.40	0.04	0.04	2.80	11.38
Tm	–	0.09	–	0.01	0.01	0.01	0.13	0.65	0.12	0.45	0.05	0.06	0.01	–	0.42	1.58
Yb	0.03	0.02	0.05	0.03	0.06	0.06	0.84	4.17	0.80	3.11	0.33	0.40	0.04	0.04	2.89	9.29
Lu	0.01	0.05	0.01	0.01	0.01	0.01	0.14	0.72	0.15	0.56	0.06	0.07	0.01	0.01	0.47	1.47
Hf	0.30	0.01	0.16	0.30	0.32	0.32	0.85	12.14	0.46	7.61	0.29	0.25	0.17	0.12	1.34	8.85
Zn	63.0	0.05	38.0	38.0	50.0	50.0	38.0	248.0	79.0	61.0	39.0	38.0	39.0	41.0	76.0	31.0
Cu	16.0	0.01	14.0	16.0	14.0	14.0	14.0	32.0	62.0	27.0	30.0	22.0	13.0	13.0	96.0	13.0
Pb	9.0	0.25	7.0	5.0	5.0	9.0	–	–	–	12.0	–	–	5.0	5.0	–	27.0
Th	0.52	41.0	0.26	0.19	5.24	0.24	2.92	19.83	0.75	8.48	0.09	0.10	0.06	0.08	0.80	17.93
U	0.06	14.0	0.08	0.31	0.51	0.08	1.08	1.54	0.04	1.10	0.05	0.05	0.37	0.09	0.07	1.70
W	0.40	–	0.32	0.26	0.41	0.57	0.44	0.44	0.28	0.52	0.49	0.62	0.95	0.99	0.46	0.38
Tl	0.07	0.31	0.05	0.17	0.25	0.05	0.12	1.09	0.15	0.50	0.03	0.07	0.05	0.03	0.10	0.75
Mo	0.72	0.06	0.47	1.02	0.33	0.66	0.11	0.63	1.16	0.70	0.62	0.40	3.99	0.51	1.16	0.67
Sn	0.60	0.28	0.60	0.40	0.50	0.60	0.60	4.10	0.90	1.90	0.70	3.30	0.80	0.40	1.20	1.00
Sb	0.26	0.05	0.40	0.35	0.43	0.81	0.24	0.29	0.14	0.16	0.85	0.27	0.16	1.16	0.19	0.32
Ga	2.0	1.41	1.0	1.0	2.0	1.0	13.0	33.0	13.0	18.0	3.0	4.0	2.0	1.0	15.0	29.0
Ge	1.0	0.60	1.0	1.0	1.0	1.0	1.3	2.3	1.7	1.6	1.2	1.8	0.9	0.9	1.9	1.7
Be	–	0.19	–	–	–	–	1.0	4.0	2.0	3.0	–	–	–	–	2.0	2.0
Ag	–	2.0	–	–	–	0.60	–	–	0.60	–	–	–	–	–	0.50	–

Abbreviations are the same as those in the Table 1. – means elements not detected.

element contents except the TC. The TC has lowest Cr (911 ppm), Co (65 ppm) and Ni (1014 ppm) contents among the four ultramafic varieties.

Incompatible element and REE; Incompatible element and REE analyses of the ultramafic rocks are presented with PM (Primitive mantle composition, from Sun, McDonough, 1989) normalized abundances in the Fig. 3 and 4, respectively. Clear geochemical distinctions are shown among the different rock types. In the PM normalized incompatible element abundances, the PD has flat patterns except Ba whereas the PSD and SP show depletions in the

high-field strength elements (HFSE) relative to the low-field strength elements (LFSE). The PSD shows higher Eu, Sr, Ba and lower Ti and Y contents than the SP. The TC shows more enrichments in the HFSE than the other rock types, but shows more depletions in HFSE than the LFSE. High Ba contents of the PD may be related to existences of the amphibole. In the PM normalized REE abundances, the PD shows flat patterns whereas the PSD and SP have HREE depleted patterns (thus, high La/Yb). The TC shows distinctive negative Eu anomaly and most enrichments in the all REE contents among the ultramafic varieties.

Others

Major and transitional elements; All major and transitional element analyses of the metabasite, gneiss and vermiculate vein samples are shown in Table 1 and 2. The metabasites show low contents of SiO_2 (46.8~48.28 wt%), and high contents of Al_2O_3 (13.9~16.3 wt%), CaO (12.9~12.3 wt%) and MgO (11.5~8.8 wt%) whereas the gneisses have high contents of SiO_2 (71.7~71.9 wt%), Al_2O_3 (13.26~11.86 wt%), and low contents of CaO (0.71~1.55 wt%), Na_2O (2.09~3.01 wt%), and MgO (1.87~1.19 wt%). The vermiculate vein shows high TiO_2 (1.08 wt%), Al_2O_3 (14.5 wt%), CaO (9.23 wt%), Na_2O (1.88 wt%), K_2O (2.04 wt%) and low MgO (7.44 wt%) contents.

The metabasites show high contents of Cr (343~466 ppm), Co (50~54 ppm), Ni (180~263 ppm), SC (33~42 ppm), V (139~288 ppm) and Zn (76~79 ppm) whereas the gneisses show low contents of Cr (60~118 ppm), Co (5~12 ppm), Ni (44~52 ppm), SC (2~12 ppm) and Zn (31~61 ppm). The vermiculate vein shows higher Ni, Cr and Co contents than the gneiss.

Incompatible element and REE; Incompatible element and REE analyses of the metabasite and gneiss are presented with PM normalized abundances in Fig. 5 and 6, respectively. In the PM normalized incompatible element abundances (Fig. 5), the metabasites show enrichments in the LFSE relative to the HFSE, but show geochemical differences between two varieties. A variety showing equigranular and mosaic textures is more depleted in the most incompatible element contents than that showing decompressive and recrystallization textures. The gneiss complexes show enrichments in the LFSE relative to the HFSE, but show enrichments in the most incompatible element contents relative to the metabasites except Sr, P and Ti. The vermiculate vein shows enrichments of the LFSE relative to the HFSE contents (Table 1, 2).

In the PM normalized REE abundances (Fig. 6), the metabasites show nearly flat patterns. However, clear differences are distinctive between two varieties. A variety showing equigranular and mosaic textures is more depleted in the all REE contents than that

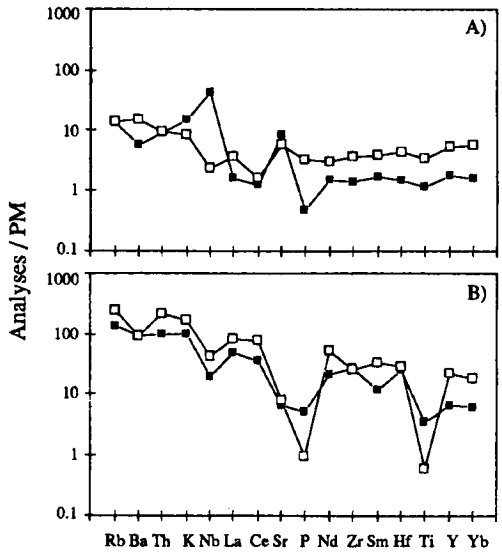

Fig. 5. PM composition normalized incompatible element abundances of metabasite (A) and gneiss (B) from adjacent to the Bibong (Filled square) and Kwangsi (Open square) ultramafic rocks. PM data from Sun and McDonough (1989).

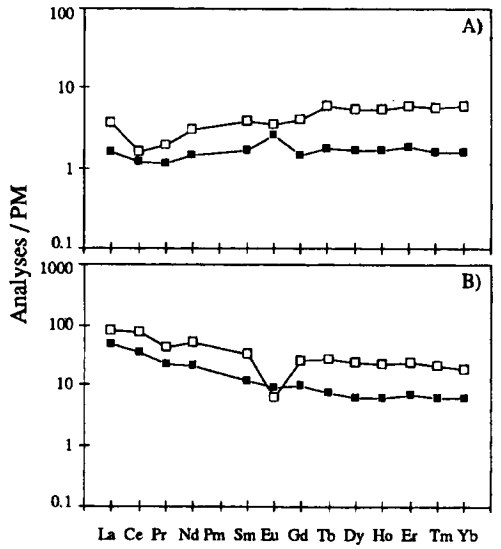

Fig. 6. PM composition normalized REE abundances of metabasite (A) and gneiss (B) from adjacent to the Bibong (Filled square) and Kwangsi (Open square) ultramafic rocks. PM data from Sun and McDonough (1989).

Table 3. Representative analyses of the olivine, pyroxene and spinel.

Mineral	olivine						Pyroxene									Spinel							
Type	PSP				PD		PSP			PD		PD		PSP	MB	PSP							
Number	BB3-4	BB4-3D	BB1-8	BB1-2	KS8-3	KS8-1	BB3-4	BB4-3D	BB1-8	KS8-3		KS8-1		BB1-	HS8-06	BB3-4	BB4-3D	BB1-8	BB1-2	BB1-9	KS8-4		BB1-9
Characteristics										Core	Rim	Core	Rim			R.B.	R.B.	R.B.	R.B.	R.B.	F.Y.	F.Y.	DA
SiO_2	41.56	41.32	40.44	41.63	41.59	41.51	57.87	59.97	57.51	55.21	57.10	55.62	59.72	54.80	51.78	–	–	–	–	–	–	–	–
Al_2O_3	–	–	–	–	–	–	0.91	1.23	1.02	3.66	1.55	4.42	2.44	0.56	2.56	35.12	35.68	26.14	43.93	31.85	55.43	50.23	3.01
TiO_2	–	–	–	–	–	–	–	–	–	–	–	–	–	–	–	–		–	–	–	–	–	–
FeO*	8.88	9.29	8.66	8.35	10.63	10.11	5.66	6.13	5.95	7.12	6.79	6.96	7.20	1.53	9.00	15.70	15.40	19.71	13.07	15.64	13.27	14.76	89.44
MgO	49.29	49.36	49.70	49.98	48.20	48.27	35.00	35.11	34.95	32.68	33.80	32.58	33.89	17.65	12.87	14.61	14.84	11.31	16.90	14.01	18.40	17.00	2.68
CaO	–	–	–	–	–	–	0.31	0.17	0.22	0.19	–	0.22	–	24.83	22.60	–	–	–	–	–	–	–	–
Na_2O	–	–	–	–	–	0.44	–	–	–	0.29	–	–	–	–	–	0.44	0.26	0.60	0.39	–	0.42	0.59	–
Cr_2O_3	–	–	–	–	–	–	–	0.31	–	0.50	–	0.43	–	–	0.81	32.59	32.12	41.11	24.32	38.20	11.97	16.59	32.45
NiO	–	0.47	0.58	–	–	–	–	–	–	–	–	–	–	–	–	–	–	–	–	–	–	–	–
Total	99.71	100.44 N(4)	99.93	99.96	100.42	100.33	99.76	100.87	99.66	99.44	99.24 N(6)	100.23	101.84	99.37	100.06	98.49	98.54	98.88	98.61	99.71 N(32)	99.49	99.17	97.57
Si	1.011	1.005	0.999	1.011	1.015	1.013	1.989	1.997	1.981	1.919	1.980	1.916	1.962	1.995	1.937	–	–	–	–	–	–	–	–
Al	–	–	–	–	–	–	0.037	0.048	0.042	0.150	0.064	0.179	0.097	0.024	0.113	9.658	9.789	7.552	11.524	8.822	13.755	12.802	0.005
Ti	–	–	–	–	–	–	–	–	–	–	–	–	–	–	–	–	0.043	–	–	–	–	–	–
Fe(2)	0.181	0.189	0.177	0.170	0.217	0.206	0.163	0.171	0.172	0.204	0.197	0.200	0.204	0.047	0.273	2.504	2.653	3.262	2.045	2.997	1.874	2.015	6.201
Fe(3)		–	–	–	–	–	–	–	–	–	–	–	–	–	–	0.501	0.310	0.702	0.349	0.071	0.416	0.588	7.093
Mg	1.796	1.791	1.810	1.809	1.754	1.757	1.793	1.745	1.795	1.696	1.748	1.673	1.711	0.958	0.718	5.078	5.148	4.135	5.608	4.911	5.776	5.483	1.132
Ca	–	–	–	–	–	–	0.011	0.006	0.008	0.007	–	0.008	–	0.969	0.906	–	–	–	–	–	–	–	–
Na	–	–	–	–	–	0.021	–	–	–	0.019	–	–	–	–	0.059	0.202	0.117	0.289	0.171	–	0.174	0.249	–
Cr	–	–	–	–	–	–	–	0.008	–	0.014	–	0.012	–	–	–	6.056	5.940	8.059	4.304	7.109	2.005	2.864	8.218
Ni	–	0.009	0.011	–	–	–	–	–	–	–	–	–	–	–	–	–	–	–	–	–	–	–	–
Mg*	90.8	90.5	91.1	91.4	89.0	89.5	91.7	91.1	91.3	89.3	89.9	89.3	89.3	95.3	72.5	67.0	66.0	55.9	73.3	62.1	75.5	73.1	15.4
Cr**																38.5	37.8	51.6	27.2	44.6	12.7	18.3	89.1

Abbreviations are the same as those in the Table 1 exclusive of following: R.B.; red brown-, F.Y.; faint yellow-, and DA; dark-colored spinels. FeO* is total iron. Fe(2) and Fe(3) contents are calculated with stoichiometry. Mg* is equal to 100×Mg/)Mg+Fe(2)) and Cr** is equal to 100×Cr/(Cr+Al). N(-) means mumber of oxygen.

showing decompressive and recrystallization textures. The gneiss complexes show more enrichment in the LREE relative to the HREE contents, but show enrichments in the most REE relative to the metabasites. The vermiculate vein shows enrichments of the LREE relative to the HREE contents (Table 1, 2).

MINERALOGY AND MINERAL CHEMISTRY OF THE ULTRAMAFIC ROCKS

Primary mineralogy

The primary mineralogy contains olivine, orthopyroxene, clinopyroxene and spinel. The olivine occurs as isolated, neoblastic or porphyroclastic (or megacrystic) grains. The megacrystic grains contain fine opaque dusty material disseminated or concentrated along the fractures whereas the neoblastic varieties do not contain opaque dusty material. Fine neoblastic grained olivines are formed from megacrystic olivines by recrystallization processes, mainly along grain boundaries and dislocations. Some of the porphy- roclastic olivine and orthopyroxene grains are rotated from the directions of the emplacements. The olivines show homogeneous, restrict compositions, ranging from Fo_{89} to Fo_{92} (Table 3). No clear compositional dif- ferences are shown among the different occurrence type of olivine. Concentrations of the minor elements are very low. All CaO, TiO_2 and Cr_2O_3 contents are in the detection limits. NiO contents of the olivine mainly range from the limit of detection to 0.5 wt%. The low Ni contents are different from olivines of cumulates and mantle peridotites (Dymek *et al.*, 1988).

The orthopyroxene occurs as isolated, neoblastic or porphyroclastic (or megacrystic) grains whereas the clinopyroxens only occur as remnant grains after replacements to amphiboles. Some megacrystic orthopyroxene grains are replaced from olivine megacrysts and enclosed by amphibole and chlorite.

The pyroxenes shows enstatitic to bronzitic (En_{88-92}) or diopsidic in compositions (Table 3). The orthopyroxenes contain wide ranges of Al_2O_3 (0.9~4.4 wt%) and low CaO (<0.31, but dominantly <0.24, wt%) contents whereas the clinopyroxens contain high CaO (24~25 wt%) contents. The lowest Al_2O_3 contents (about 0.91 wt%) are shown in the marginally replaced grains by chlorites. The ortho- pyroxene megacrysts are zoned in aluminium contents (high Al_2O_3 in the core (> 3.5 wt%) and low in the rim (<1.6 wt%)). The neoblastic grains are also low Al_2O_3 and CaO contents. The highest Al_2O_3 contents in the their core may reflect equilibration with primary mineralogy, olivine and spinel (Dymek *et al.*, 1988). The low Al_2O_3 and CaO contents in the orthopyroxene are similar to those from contact metamorphosed (Arai, 1972) and regionally metamorphosed peridotites (Evans, Trommsdorff, 1974). The low contents of aluminium and calcium are characteristics of the orthopyroxenes in the amphibolite facies metamorphic rocks (Evans, 1977). On the other hand, high aluminous orthopyroxenes are well known in alpine spinel peridotites equilibrated in the granulite facies (Evans, 1978).

The spinels mainly occur as isolated and as replaced grains of olivines. The former can be considered as primary grains. They are spinel or range from magnesio-chromite to chromite in compositions (Table 3, Fig. 7). The chromites mainly show zonal textures, magnesio-chromite in the core and chromite in the rim. The spinel show faint yellow in color whereas magnesio-chromite and chromite show red brown and dark, respectively.

The spinels have high Al_2O_3 (54~57 wt%), MgO (18~19 wt%) and moderate Cr_2O_3 (3~14 wt%) contents. The magnesio-chromites contain moderate Al $_2O_3$ (26~44 wt%), MgO (12~15 wt%) and high Cr_2O_3 (24~41 wt%) contents whereas the chromites contain high Cr_2O_3 (27~33 wt%), and low Al_2O_3 (2~3

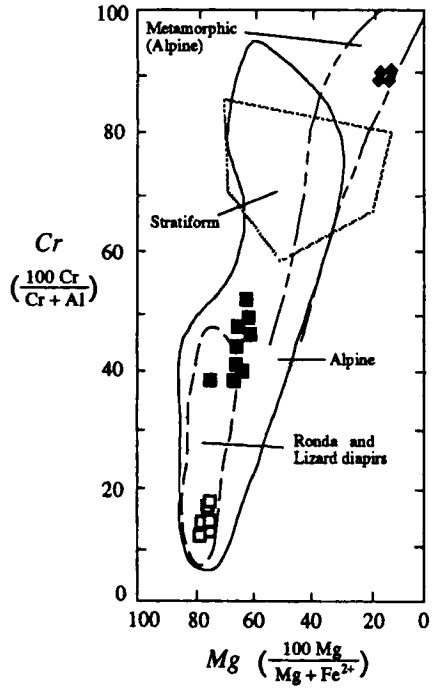

Fig. 7. Plot of spinel compositions of the ultramafic rocks from the Bibiong area and their comparisons with available data. Data from Dick, Bullen (1984), Lipin (1984) and A-gata (1988). Filled square for red brown-, open square for faint yellow, and filled diamond for darkcolored spinels.

wt%) and MgO (1.5~3 wt%) contents. The spinels from the Bibong area are similar to those from the alpine type ultramafic rocks in compositions (Dick, Bullen, 1984; Lipin, 1984; Agata, 1988) (Fig. 7).

Serpentinite mineralogy

The serpentinite minerals contain seperntine, talc, chlorite, hornblende, calcite and magnetite.

The serpentines are antigorite, lizardite, and chrysotile. They may be distinguished by their textures (Wicks, Whittaker, 1977; Wick, O'Hanley, 1988). Antigorite tends to form interpenetrating to interlocking textures composed of elongated blades and plates. Lizardite occurs along the olivine grain boun- daries or fractures and commonly forms pseudo- morphic "mesh" textures after olivine. Chrysotile tends to form cross-fibers or ribbon textures. Small amounts of chrysotile present in lizardite mesh textures after olivine. The chemical differences between antigorite and lizardite/chrysotile are small (Peacock, 1987), but can be discerned with the electron microprobe. Antigorites show slightly lower MgO, H_2O and higher SiO_2 than lizardite/chrysotile as mentioned by Peacock (1987) in a study of the Trinity peridotite, northern California.

However in the Bibong area, no clear chemical differences are found among the ultramafic textural varieties (Table 4). Generally, serpentine showing remnants of host olivine grains have slightly higher Al_2O_3 than adjacent serpentine absolutely altered (Table 4).

The amphiboles plot between tremolite and pargasite end members (Fig. 8). More tremolitic grains are colorless and occur as commonly elongated grains whereas the pargasitic grains mainly show light green and occur as subhedral to euhedral grains. Some amphibole replaces orthopyroxene megacrysts.

Generally, amphiboles have high concentrations of Al_2O_3 (9.9~12.3 wt%) and Cr_2O_3 (0.8~1.6 wt%) (Table 4). The pargasitic hornblendes occur as results of alkali-metasomatism whereas the tremolitic hornblendes are mainly crystallized under isochemical condition of metamorphism (Deer *et al.*, 1962). As shown in Fig. 8, calcic amphibole composition of the ultramafic rocks from the Bibong area are plotted in the field of

Table 4. Representative analyses of the calcic amphibole, chlorite and serpentine.

Mineral	calcic amphibole						Chlorite				Serpentine				
Type	PSP		PD			MB	PSP		PD		PSP				
Number	BB1-8	BB1-2	KS8-3	KS8-1		HS8-6	BB1-2	BB3-4	KS8-1		BB3-4	BB4-3B	BB1-8	BB1-9	KS8-1
SiO_2	49.60	45.73	48.22	49.70	51.62	42.29	32.28	35.36	29.90	29.36	44.48	42.07	43.32	43.75	40.78
Al_2O_3	10.86	11.72	11.68	10.26	8.17	13.50	8.24	9.16	19.10	19.28	0.32	0.56	–	–	0.69
TiO_2	0.25	0.31	0.60	0.48	–	0.37	–	0.26	–	0.21	–	–	–	–	–
FeO*	2.51	2.77	3.15	3.36	2.87	0.74	2.67	6.51	3.24	3.45	1.60	2.69	1.91	1.10	5.12
MgO	19.42	18.92	19.82	19.55	20.64	11.39	34.69	32.85	30.72	31.10	39.86	38.63	40.44	40.19	36.02
CaO	12.82	12.79	12.90	12.62	12.80	11.41	–	–	–	–	–	0.20	–	–	0.17
Na_2O	1.94	1.96	2.04	1.60	1.44	2.94	0.28	–	–	–	–	–	–	–	–
K_2O	0.77	0.73	0.15	–	0.34	–	–	0.16	–	–	–	–	–	–	–
Cr_2O_3	0.95	1.40	0.80	0.90	0.87	0.52	1.19	0.47	1.26	1.37	–	–	–	–	–
NiO	–	–	–	–	–	–	–	–	–	–	–	–	–	–	–
Total	96.42	96.33	98.45 N(23)	98.48	98.62	97.15	84.34	85.77	84.17 N(28)	85.26	88.25	84.14	85.69 N(14)	85.05	82.48
Si	6.653	6.508	6.689	6.828	7.061	6.167	6.707	6.923	5.831	5.766	41.44	4.057	4.083	4.129	4.038
Al	1.815	1.969	1.910	1.652	1.714	2.320	2.018	2.113	4.390	4.389	0.035	0.062	–	–	0.081
Ti	0.026	0.034	0.058	0.049	–	0.044	–	0.038	–	0.030	–	–	–	–	–
Fe(2)	0.146	0.129	0.302	0.142	0.035	1.078	0.464	1.06	0.528	0.568	0.124	0.217	0.150	0.087	0.427
Fe(3)	0.152	0.204	0.064	0.244	0.294	0.841	–	–	–	–	–	–	–	–	–
Mg	4.106	4.011	3.912	3.984	4.208	2.471	10.747	9.588	8.934	8.954	5.536	5.555	5.684	5.656	5.356
Ca	1.951	1.950	1.918	1.849	1.875	1.779	–	–	–	–	–	0.020	–	–	0.018
Na	0.537	0.498	0.551	0.427	0.378	0.832	–	–	–	–	–	–	–	–	–
K	0.136	0.137	0.025	0.131	0.059	–	–	0.290	–	–	–	–	–	–	–
Cr	0.102	0.154	0.083	0.099	0.092	0.061	0.195	0.073	0.189	0.208	–	–	–	–	–
Ni	–	–	–	–	–	–	–	–	–	–	–	–	–	–	–

Abbreviations are the same as those in the Table 1. FeO* is total iron. Fe(2) and Fe(3) contents are calculated with a program, ENP-AMPH (Mogessie *et al.*, 1988). N(-) means number of oxygen.

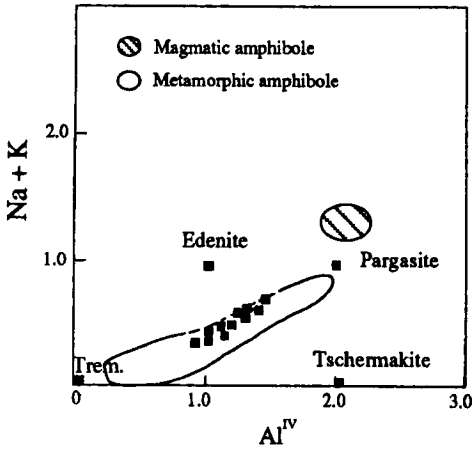

Fig. 8. Plot of Al(4) versus Na+K (Number of atoms per 23 oxygen atoms) in calcic amphibole of the ultramafic rocks from the Bibiong area. Locations of end member compositions are after Deer *et al.* (1966). Fields of metamorphic and magmatic amphiboles are from those of Jamieson (1981).

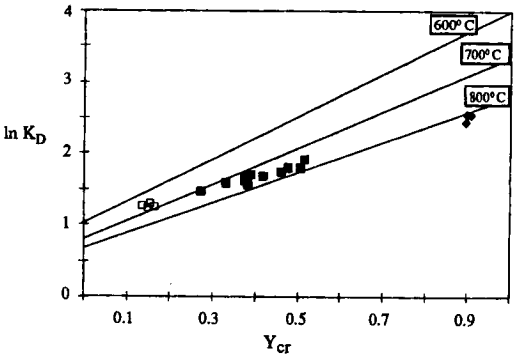

Fig. 9. Plot of ln KD versus YCr. In KD=(X_{Mg}/X_{Fe})ol* (X_{Fe}/X_{Mg})sp, Y_{Cr}=(Cr/(Cr+Al). Solid lines are the isotherms calculated from the equation of Fabries (1979). Symbols are in the Fig. 7.

metamorphic amphiboles defined by Jamieson (1981).

The chlorites are typically colorless with anomalous brown birefringence and are clinochore, penninite or talc-chlorite in compositions according to the classification of Deer *et al.* (1962) (Table 4). They occur as coronas of pyroxene and along the fracture or rim of amphibole.

The magnetites occur as relicts of olivine and pyroxene or their fractures, or rim of chromites. The talcs are colorless to very light brown in color and occur as subhedral tabular grains. The grains occur in three distinct forms; 1) disseminated throughout the rocks; 2) confined to veins; and 3) related to the alteration of tremolite suites. The other grains are calcite, magnesite and dolomite.

GEOTEMPERATURE ESTIMATES

Olivine-spinel geothermometry based on the partitions of Mg and Fe^{2+} between coexisting spinel and olivine has been applied to ultramafic rocks from the Bibong area (Fig. 9). This study has adopted to use the equation of Fabries (1979), which yields internally consistent equilibration temperatures between those calculated using the methods of Sack (1982) and Engi (1983). Alteration temperatures of the ultramafic rocks from the Bibong area using olivine-spinel geothermometry of Fabries (1979) are vary from 640°C to 810°C (Fig. 9). Of the zoned grains, chromites shown as the core range from 740°C to 770°C whereas magnesio-chromites shown as the rim range from 640°C to 690°C. In contrast to them, alteration temperatures of spinels range from 800°C to 820°C. Assuming that olivines equilibrated with core as well as rim in the zoned spinel grains, the geothermometry may represent the retrogressive metamorphism in a condition ranging from the upper amphibolite facies to greenschist facies.

DISCUSSIONS

Occurrences

As mentioned above, the ultramafic rocks from the Bibong area show high *Mg*, and high Ni, Co and Cr, low alkali K_2O and Na_2O contents (Table 1, 2). They also show enrichments in the LFSE relative to the HFSE contents and depletion in the REE contents (Fig. 10). Olivine contents of the ultramafic rocks show high *Mg* (>87), which are equilibrated with upper mantle peridotites (Irving, Green, 1976).

The mineralogical and geochemical compositions are similar to those of ultramafic xenoliths within the alkaline basalts, eastern Australia (Griffin *et al.*, 1988; O'Reilly, Griffin, 1988; McDonough *et al.*, 1990) and orogenic related ultramafic rocks from western Alps (Bodinier, 1988) and Isua, western Greenland (Dymek *et al.*, 1988). The worldwide studies suggest that the ultramafic rocks have high *Mg*, transitional element, low alkali and depleted REE contents in whole rock compositions, and high *Mg* in olivine compositions.

Occurrences of the alpine type ultramafic rock have been mentioned by several authors (Hess, 1955; Moore, MacGregor, 1972; Moores, 1973; Hoogerduijn *et al.*, 1993; Ozawa, 1994; Rampone *et al.*, 1995;

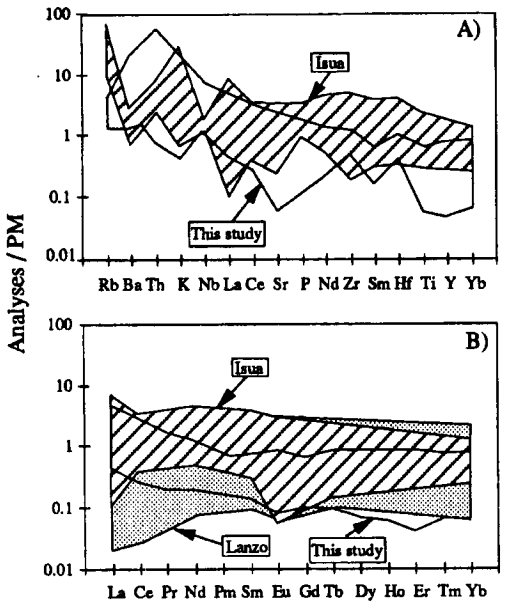

Fig. 10. PM composition normalized incompatible element and REE abundances of the ultramafic rocks from the Bibong area and their comparisons with available data. Data; Isua from Dymek *et al.* (1988), Lanzo from Bodinier (1988). PM data from Sun, McDonough (1989).

Raymond, 1995). Their general agreements of the petrogenetic types are three opinions; A) magmatic differentiates (Maaloe, Steel, 1980; Menzies, 1984; Irfune, Ringwwod, 1987; Bodinier, 1988; Casey *et al.*, 1983), B) mantle slabs (Quick. 1981; Sarwat, DeJond, 1984; Raymond, 1995) and C) mantle diapirs (Loomis, 1972; Dymek *et al.*, 1988).

The type (A) shows characteristics of the type of igneous protolith from which they were derived, such as dominant or relict igneous textures, primary layering in some bodies, and mafic and felsic differentiates associated with the ultramafic bodies whereas the type (C) produces a contact metamorphic aureole in the adjacent host rock because the alpine type ultramafic rocks are emplaced at high temperatures.

However, the type (B) is subcrustal mantle which is faulted into the crust. It dominantly shows protogranular, equigranular-mosaic and equigranular-tabular textures. It has high *Mg*, moderate CaO and Al_2O_3 contents in the whole rock compositions and high fosterite contents in olivine, MgO in orthopyroxene, and high Cr/(Cr+Al) ratios in Cr-spinel (Raymond *et al.*, 1995).

At the Bibong area, the ultramafic rocks occur with adjacent Precambrian gneiss complex as the steeply dipping fault. No contact metamorphic aureole as shown the type (C) are found in the adjacent metamorphic rocks. On the microscope, the fresh ultramafic masses (especially, PD and PSP) show protogranular, equigranular-mosaic and equigranular-tabular textures. No cumulate fabrics are found. They have high magnesium number, low Al_2O_3 and moderate CaO contents in the whole rock compositions and contain mineral composition showing high contents of fosterite in the olivine, of MgO in orthopyroxene and of Cr in the spinel.

In summary, overall characteristics of the ultramafic rocks from the Bibong area suggest that their occurrences are similar to those shown at ultramafic rocks which were emplaced into the crust by the faulting as mantle slab types.

CONCLUSIONS

1. The Bibong and Kwangsi ultramafic rocks occur as discontinuous isolated lenticular bodies to NNE directions which are parallel to fault lines of the Precambrian Kyeonggi gneiss complex. They contact with the adjacent gneiss complex as steeply dipping faults.

2. The ultramafic rocks are dunites and harzburgites and many of them are partially or completely serpentinized. They contain varying amounts of olivine (Fo_{90-92}), enstatitic to bronzitic orthopyroxene, diopsidic clinopyroxene, tremolitic to pargasitic hornblende, and spinel with serpentine, talc, chlorite, calcite and magnetite. The rocks dominantly show protogranular, equigranular-mosaic and equigranular-tabular textures. Some of them show porphyroclastic (megacrystic) and recrystallized textures, reflecting several stages of metamorphism.

3. The ultramafic rocks show high magnesium number (>89), and transitional element (Ni>2400, Co>100, Cr>1700 ppm) and low alkali (K_2O<0.03 wt%, Na_2O<0.24 wt%) contents and depleted REE patterns. Of the ultramafic rock varieties, peridotites show lower LREE/HREE, and LFSE/HFSE ratios than partly serpentinized ultramafic rocks whereas talcified rocks are enriched in the most of incompatible element relative to the other types.

4. Mineralogical and geochemical comparisons with available data, high *Mg*, transitional and low alkali element, and depleted REE contents shown in the Bibong and Kwangsi ultramafic rocks are similar to those of worldwide mantle xenoliths and alpine type ultramafic rocks.

5. Overall characteristics of the field evidences, petrographical, geochemical and mineralogical characteristics shown in the Bibong and Kwangsi

ultramafic rocks suggest that they are similar to those emplaced into the crust by the faulting as mantle slab types.

6. With distinctive petrographical characteristics, mineralogical compositions of the ultramafic rocks such as low Ni contents in olivine, and low aluminium and calcium contents in the orthopyroxene are similar to those of worldwide metamorphosed tectonic related ultramafic rocks.

7. Calculated temperature, using olivine and spinel geothermometry, with mineralogical characteristics suggest that the ultramafic rocks of the Bibong area have metamorphosed in a condition ranging from the upper amphibolite facies to greenschist facies.

ACKNOWLEDGEMENTS

Financial research grant for this study was provided by the Center for Mineral Resources Research sponsored by the Korea Science and Engineering Foundation, and Korea Research Foundation for Post-Doc program which is greatly acknowledged.

REFERENCES

Agata, T. (1988) Chrome spinels from the Oura layered igneous complex, central Japan. Lithos, v. 21, 284, p. 350-375.

Aray, S. (1972) An estimation of the last depleted spinel peridotite on the basis of olivine-spinel mantle array. Neues. Jahrb. Fur. Miner. Minatsh, v. 8, p. 347-354.

Bodinier, J.L. (1988) Geochemistry and petrogenesis of the Lanzo peridotite body, western Alps. Tectnophy., v. 149, p. 67-88.

Boyd, F.R., Green, D.H. and Roy, S.D. (1978). Origin of the ultramafic nodules from some kimberlites of northern Lesotho and Monastery Mine, South Africa. Phys. Chem. Earth., v. 9, p. 431-454.

Casey, J.F., Karson, J.A., Elthon, D., Rosencrantz, E. and Titus, M. (1983) Reconstruction of geometry of accretion during formation of the bay of Islands ophiolite complex. Tectonphy., v. 116, p. 509-528.

Choi, S.Y. (1988) A study on the origin of the serpentinite in the Ulsan mine area, PhD thesis in Pusan National Univ. (Unpublished).

Christensen, N.I. and Lundquist, S.M. (1982). Pyroxene orientation within the upper mantle., Geol. Soc. Amer. Bull., v. 93, p. 279-288.

Deer, W.A., Howie, R.A. and Zusmann, J. (1962) Rock forming mineral. Longmans, p. 173-174.

Den Tex, E. (1969) Origin of ultramafic rocks, their tectonic setting and history: A contribution to the discussion of the paper "The origin of ultramafic and ultrabasic rocks" by P. J. Wyllie. Tectonophy., v. 7, p. 457-488.

Dick, H.J.B. and Bullen, T. (1984) Chromian spinel as a petrogenetic indicator in abyssal and Alpine-type peridotites and spatially associated lavas. Contrib. Miner. Petrol., v. 86, p. 54-76.

Dymek, R.F., Brothers, S.C. and Schiffries, C.M. (1988) Petrogenesis of ultramafic metamorphic rocks from 3800 Ma Isua supracrustal belt, western Greenland, J. Petrol., v. 29, p. 1353-1397.

Engi, M. (1983) Equilibria involving Al-Cr spinel: Mg-Fe exchange with olivine. Experiments, Thermodynamic analysis, and consequemces for geothermometry. Am. J. Sci., 283A, p. 29-71.

Eum, S.H. and Lee, M.S. (1963) Geological map of Daehung area. 1/50000. Inst. Geol. Surv. Korea, p. 1-17.

Evans, B.W. (1977) Metamorphism of alpine peridotite and serpentinite. Ann. Rev. Earth Planet Sci., v. 5, p. 397-447.

Evans, B.W. (1978) Metamorphism of the Alpine peridotite and serpentinite. Ann. Rev. Earth Planet Sci., v. 5, p. 397-447.

Evans, B.W. and Trommsdorff, V. (1974) Stability of enstatite+ talc and CO2 metasomatism of metaperidotite, Val d'Efra, Lepontine Alps. Amer. J. Sci., v. 274, p. 274-296.

Fabries, J. (1979) Spinel-olivine geothermometry in peridotites from ultramafic complexes. Contrib. Miner. Petrol., v. 69, p. 329-336.

Frey, F.A. and Green, D.H. (1974) The mineralogy, geochemistry and origin of lherzolite inclusion in Victorian basanites. Geochim. Cosmochim. Acta, v. 38, p. 1023-1059.

Girardeau, J. and Mercier, J.C.C. (1988) Petrology and texture of the ultramafic rocks of the Xigaze ophiolite (Tibet): Constraints for mantle structure beneath slow-spreading ridges. Tectonophy., v. 147, p. 33-58.

Griffin, W.L., Wass, S.Y. and Hollis, J.D. (1984) Ultramafic xenoliths from Bullenmerri and Gnotuk Maars, Victoria, Australia: petrology of sub-continental crust-mantle transition. J. Petrol., v. 25, p. 53-89.

Griffin, W.L., O'Reilly S.Y. and Stabel, A. (1988) Mantle metasomatism beneath western Victora, Australia: II. Isotopic geochemistry of Cr-diopside lherzolites and Al-augite pyroxenite. Geochim. Cosmochim. Acta, v. 52, p. 449-460.

Hamlyn, P.R. and Bonatti, E. (1980) Petrology of mantle derived ultramafic rocks from the Owen Fracture Zone. northwest Indian Ocean: Implications for the nature of the oceanic upper mantle. Earth Planet Sci. Lett., v. 48, p. 65-79.

Hebert, R., Serri, G. and Hekinian, R. (1989) Mineral chemistry of ultramafic tectonites and ultramafic to gabbroic cumulates from the major oceanic basins and northern Apennine ophiolites (Italy): A comparison. Chemical Geol., v. 77, p. 183-207.

Hess, H.H. (1955) Serpentines, orogeny, and epiogeny. In Polervaart, A., (ed.), Crust of the Earth. Geol. Soci. Amer. Spec. Pap., no. 62, p. 391-407.

Hoogerduijn S.E.H., Rampone, E., Piccardo, G.B., Drury, M. R. and Vissers, R.L. (1993) Subsolidus emplacement of mantle peridotites during incipent oceanic rifting and opening of the Mesozoic Tethys (Voltri Massif, NW Italy). J. Petrol., v. 34, p. 901-927.

Hwang, J.Y., Kim, J.K. and Ock, S.S. (1993) Genesis and Mineralogy of the serpentinite deposits inn the Andong area, Korea. J. Korean Inst. Min. Geol., v. 26, p. 1-10.

Irifune, T. and Ringwood, A.E. (1987) Phase transformations in a dynamical behavior of the subduction slab. Earth

Planet. Sci. Lett., v. 86, p. 367-376.

Irving, A.J. and Green, D.H. (1976) Geochemistry and petrogenesis of the New basalts of the Victoria and South Australia. J. Geol. Soc. Aust., v. 23, p. 45-66.

Jackson, I. (1991) The petrological basis for the interpretation of seismological models for continental lithosphere. In Drummond, B.J. (ed.), The Eastern Australian lithosphere. Geol. Soc. Aust. Spec. Pub., v. 17, p. 81-114.

Jamieson, R.A. (1981) Metamorphism during ophiolite emplacement- the petrology of the St. Anthony Complex. J. Petrol., v. 22, p. 397-449.

Ji, J.M. and Kim, K.B. (1977) A study of talc mineralization of serpentine. J. Korea. Inst. Min. Geol., v. 10, p. 67-74.

Kim, K.H., Park, J.K., Yang, J.M. and Yoshida, N. (1990) Petrogenesis of the carbonate and serpentinite rocks from the Ulsan iron mine. J. Geol. Soc. Korea, v. 26., p. 407-417.

Lee, C.H. and Kim, S.S. (1963) Geological map of Hongseong area. 1/50000. Inst. Geol. Surv. Korea, p. 1-31.

Lipin, B.R. (1984) Chromite from the Blue Ridge province of North Calorina. Amer. J. Sci., v. 284, p. 507-529.

Loomis, T.P. (1972) Diapiric emplacemet of the Ronda high-temperature ultramafic intrusion, southern Spain. Geol. Soc. Amer. Bull., v. 83, p. 2475-2496.

Maaloe, S. and Steel, R. (1980) Mantle composition derived from the composition of lherzolites. Nature, v. 285, p. 321-322.

McDonough, W.F. (1990) Constraints on the composition of the continental lithospheric mantle. Earth Planet. Sci. Lett., v. 101, p. 1-18.

Menzies, M.A. (1984) Chemical and isotopic heterogeneities in orogenic and ophiolitic peridotites. In Gass, I.G., Lippard, S.J. and Shelton, A.W. (ed.), Ophiolites and Oceanic Lithosphere. Blackwell, Sci. Pubs. Geol. Soc. (London) Spec. Pub., no. 13. p. 231-240.

Mittsede, S.K. and Stoddard, E.F. (1989) Ultramafic Rocks of the Appalachian Piedmont. (ed.) Geol. Soc. Amer. Spec. Pub., no. 231, 103 p.

Moores, E.M. (1973) Geotectonic significance of ultramafic rocks. Earth Science Rev., v. 9, p. 241-258.

Moores, E.M. and Jackson, E.D. (1974) Ophiolites and oceanic crust. Nature, v. 250, p. 136-138.

Moores, E.M. and MacGregor, I.E. (1972) Types of alpine ultramafic rocks and their implications for fossil plate interactions. In Shagam, R. *et al.*, (ed.), studies in Earth and Space Sciences. Geol. Soc. Amer. Memor, no. 132, p. 209-223.

Nicolas, A. (1986) Structure and petrology of peridotites: Clues to their geodynamic environment. Rev. Geophys., v. 24, p. 875-895.

Nicolas, A. and Viollete, J.F. (1982) Mantle flow a oceanic spreading centers: Models derived from ophiolites. Tectonphy., v. 81, p. 319-339.

Nutman, A.P., Allaart, J.H., Bridgewater, D., Dimoroth, E. and Rosing, M. (1984) Stratigraphic and geochemical evidence for depositional environment of the early Archaean Isua Supracrustal belt, southern West Greenland. Precam. Res., v. 25, p. 365-396.

O'Reilly, S.Y., Griffin, W.L. and Stable, A. (1988) Evolution of Phanerozoic eastern Australia: isotopic evidence for miasmatic and tectonic underplating. In: Menzies, M.A. and Cox, K.G. (ed.), Oceanic and continental lithosphere: similarities and differences. J. Petrol. Spec. Publ., p. 89-108.

O'Reilly, S.Y. and Griffin, W.L. (1988) Mantle metasomatism beneath western Victoria, Australia: I. Metasomatic processes in Cr-diopside lherzolites. Geochim. Cosmochim. Acta, v. 52, p. 433-447.

Oterdoom, W.H. (1978) Tramolite and diopside-bearing serpentinite assemblages in the CaO, MgO, SiO_2, H_2O multisystem. Schweiz. Miner. Petrol. Mitt., v. 58, p. 127-138.

Ozawa, K. (1994) Melting and melt segregation in the mantle wedge above a subduction zone: Evidence from the chromite-bearing peridotites of the Miyamori ophiolite complex, Northeastern Japan. J. Petrol., v. 35, p. 647-678.

Paktung, A.D. (1984) Metamorphism of the ultramafic rocks of the Thompson mine , Thompson nickel belt, Northern Manitovia. Canadian Miner., v. 22, p. 77-91.

Peacock, S.M. (1987) Serpentinization and infiltration metasomatism in the Trinity peridotite, Klamath province, northern California: implications for subduction zones. Contrib, Miner. Petrol., v. 95, p. 55-70.

Quick, J.E. (1981) The origin and significance of large, tabular dunite bodies in the Trinity peridotite, northern California. Contrib. Miner. Petrol., v. 78, p. 413-422.

Rampone, E.M., Hofmann, A.W., Piccardo, G.B., Vanuggi, R., Bottazzi, P. and Ottolini, L. (1995) Petrology, mineral and isotope geochemistry of the external Liguride peridotites (Northern Apennines, Italy). J. Petrol., v. 36, p. 81-105.

Raymond, L.A. (1995) Metamorphic petrology, Wm. C. Brown Publishers, p. 656-675.

Sack, R.O. (1982) Spinels as petrogenetic indicators; activity-composition relations at low pressure. Contrib. Miner. Petrol., v. 79, p. 169-186.

Sarwat, G. and DeJong, K. (1984) Composition and origin of the Kanar Melange, southern Parkistan. In Raymond, L. A., (ed.), Melange: Their nature, Origin and Significance, Geol. Soc. Amer, Spec. Pap., no. 198, p. 127-138.

Song, Y. and Moon, H.S. (1991) Supergene chloritization and vermiculitization in hornblende gneiss, the Cheongyang area. J. Korean Inst. Mining Geol., v. 24, p. 233-244.

Spell, T.L. and Norrell, G.T. (1990) The Ropes Creek assemblage: Petrology, geochemistry and tectonic setting of an ophiolitic thrust sheet in the southern Appalachians. Amer. J. Sci., v. 290, p. 811-842.

Sun, S.S. and McDonough, W.F. (1989) Chemical and isotopic systematics of oceanic basalts: implications for mantle composition and processes. In Saunders, A. D. and Norry, M. J. (ed.), Magmatism in the Ocean Basins. Geol. Soc. Spec. Publ., 42, 313-345.

Wee, S.M., Choi, S.G. and So, C.G. (1994) Preliminary study on ultramafic rocks from the Chungnam Province, Korea. Econ. Environ. Geol., v. 27, p. 171-180.

Wicks, F.J. and Whittaker E.J.W. (1977) Serpentine textures and serpentinization. Can. Miner., v. 15, p. 459-488.

Wick. F.J. and O'Hanley, D.S. (1988) Serpentiine minerals: structures and petrology. In Baily, S. W. (ed.), Hydrous Phyllosilicates (exclusive of micas). Rev. Miner., v. 19, p. 91-168.

Woo, Y.K., Choi, S.W. and Park, K.H. (1991) Genesis of talc

ore deposits in the Yesan area of Chungnam, Korea. Jour. Korean Inst. Min. Geol., v. 24, p. 363-378.

Yun, S.P., Moon, H.S. and Song, Y. (1994) Mineralogy and Genesis of the Pyoungan and Daeheung Talc Deposits in Ultramafic Rocks, the Yoogoo Area. Econ. Environ. Geol., v. 27, p.131-145.

Manscript received 9 September 1997

경기편마암복합체내 비봉지역에 분포하는 초염기성암에 대한 성인적 적용

송석환 · 최선규 · 우준기

요 약 : 충남 비봉지역에서 산출되는 초염기성 암체는 경기편마암복합체내에 북북동 방향을 따라 200 m 연장을 갖고 국부적으로 산출되고 있으며, 주변 편마암체와 주로 단층접촉을 하며 평행하게 분포하고 있다. 초염기성암은 대부분 듀나이트와 하즈버가이트이며 부분 또는 완전히 사문암화되었다. 본 암석은 원생입상, 등립입상 및 등립입상-모자이크 조직을 보이며 부분적으로는 변성작용을 반영하는 잔쇄반상(잔쇄거정질) 조직 및 여러시기의 재결정 흔적을 보인다. 이 암석은 감람석 (Fo_{89-92}), 엔스테타이트에서 브론자이트 조성의 사방휘석, 투휘석 조성의 단사휘석, 투각섬석에서 파가사이트 조성의 각섬석, 첨정석, 그리고 사문석, 활석, 녹리석, 방해석, 자철석등을 포함한다. 이 초염기성암은 마그네슘비가 높고, 알칼리 이온의 함량이 낮으며 희토류원소가 결핍된 특징을 보인다. 이런 지화학적, 광물학적 특징은 전세계의 맨틀포획암 및 구조적으로 지표면에 노출된 초염기성암과 유사하다. 암석의 산상 및 암석학적, 광물학적, 지화학적 특징은 이 초염기성암의 산상이 맨틀슬랩형으로 단층작용에 의해 지표면에 정치된 알파인형 (alpine type)의 초염기성암과 유사하다. 암석학적 특징과 함께 광물 조성은 비봉지역의 초염기성암이 상부 각섬암상부터 녹색편암상 범위에서 수회의 후퇴변성작용을 받았음을 암시한다.